Acta Crystallographica Section B
Structural Science
ISSN 0108-7681

Hexamer formation in tertiary butyl alcohol (2-methyl-2-propanol, $C_4H_{10}O$)

Pamela A. McGregor,[a] David R. Allan,[a]* Simon Parsons[a] and Stewart J. Clark[b]

[a]School of Chemistry, The University of Edinburgh, Edinburgh EH9 3JJ, Scotland, and [b]Department of Physics, The University of Durham, Science Laboratories, South Road, Durham DH1 3LE, England

Correspondence e-mail: d.r.allan@ed.ac.uk

Received 27 October 2005
Accepted 27 April 2006

The crystal structure of phase II of tertiary butyl alcohol (2-methyl-2-propanol, $C_4H_{10}O$) has been solved using a combination of single-crystal X-ray diffraction techniques and *ab initio* density functional calculations. This trigonal $P\overline{3}$ phase, which is stable at both low temperature and high pressure, and the triclinic $P\overline{1}$ phase (phase IV) have very similar enthalpies, the calculations revealing only a 3.859 kJ mol^{-1} enthalpy difference at ambient pressure, despite the substantial change of the intermolecular bonding motif from helical catemer to hexamer with an increase in pressure or reduction in temperature. The hexamers in the trigonal phase adopt a chair conformation. There are two unique hexamers: at low temperature these are centred at (0, 0, $\frac{1}{2}$) and ($\frac{2}{3}$, $\frac{1}{3}$, 0.961 (13)), and at high pressure the centres are (0, 0, $\frac{1}{2}$) and ($\frac{2}{3}$, $\frac{1}{3}$, 0.958 (14)). A slight flattening of the hexamers is observed at high pressure and the calculations confirm that phase II becomes more stable relative to phase IV on pressure increase.

1. Introduction

The study of the structural systematics of small-molecule systems is rewarding as they reveal trends in whole classes of compounds and larger molecular systems. Brock & Duncan (1994) have described the general features of the packing motifs adopted by mono-alcohols (*R*OH) where there is a competition between the packing requirements of the relatively bulky *R* group and the need for the small hydroxyl groups to be close enough to form hydrogen bonds. If the molecules are relatively small then they can form catemers, generated by either a glide plane or a 2_1-screw axis, where the molecules form an approximately coplanar alternating sequence about the central chain of hydrogen bonds. If the molecules contain larger *R* groups, steric hindrance often prohibits this simple arrangement and, instead, the molecules often form chains about three-, four- or sixfold screw axes, or adopt crystal structures with more than one molecule in the asymmetric unit. Molecules containing particularly bulky *R* groups may no longer form hydrogen-bonded chains or catemers, but cyclic dimer, trimer, tetramer or hexamer rings can be created. We have been investigating the high-pressure polymorphism of a range of prototypical monoalcohols including methanol (Allan *et al.*, 1998), ethanol (Allan & Clark, 1999; Allan *et al.*, 2001), phenol (Allan *et al.*, 2002) and its halogenated derivatives (*e.g.* 2-chlorophenol and 4-fluorophenol) (Oswald, Allan, Day *et al.*, 2005; Oswald, Allan, Motherwell & Parsons, 2005), and, more recently, cyclobutanol (McGregor *et al.*, 2005) and cyclopentanol (Moggach *et al.*, 2005), with a view to establishing trends in their packing and hydrogen-bonding behaviour. In general, we find that

© 2006 International Union of Crystallography
Printed in Great Britain – all rights reserved

pressure tends to transform the packing of the *R* groups from having characteristics more closely associated with bulky groups to those more typical of small groups: *i.e.* pressure tends to promote catemers with a simple alternating sequence of molecules rather than the formation of helical chains or rings. Here we have extended our range of studies to tertiary butyl alcohol (*t*-butanol, $C_4H_{10}O$), which has the bulkiest *R* group of all the monoalcohol systems we have investigated to date.

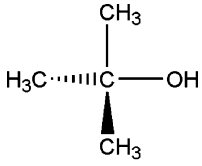

The low-temperature behaviour of *t*-butanol in the solid state has been studied using a variety of techniques, including calorimetry, spectroscopy, neutron scattering and X-ray diffraction (Steininger *et al.*, 1989). In the calorimetric measurements of Oetting (1963), three crystalline phases were noted, although their structures were not determined. It was found that phase II is stable below 281 K and, from their IR studies, Sciesinska & Sciesinska (1980) concluded that the crystal structure contains hydrogen-bonded chains of molecules. Phase II was found to transform into either phase I at 286.14 K or phase III at 281.54 K; the latter was reported to have a milky appearance and was stable between approximately 282 and 295 K. Although Steininger *et al.* (1989) reported that it is difficult to grow single crystals of phase III, they found that needle-like single crystals of phase I could be formed readily if the melt was supercooled in the temperature range between 281 K and the melting point at 298.97 K. The IR work of Sciesinska & Sciesinska (1980) indicates that the structure of phase I is likely to be formed from 'curl-like' disordered hydrogen-bonded chains (Steininger *et al.*, 1989). Dilatometric studies by Neu (1968) show that a further phase of *t*-butanol exists as the density of a sample of phase I increases with time if it is stored at 298 K.

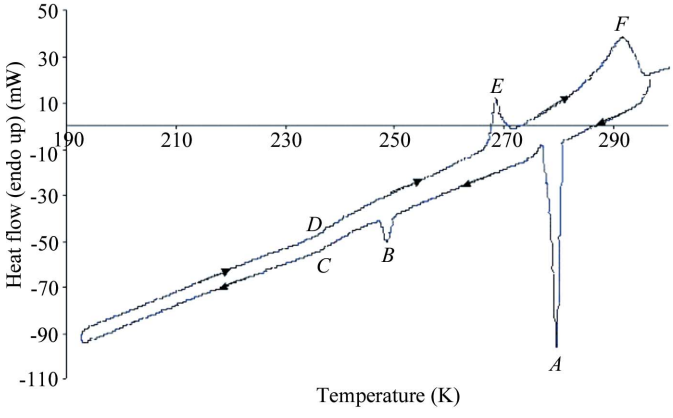

Figure 1
Graph of heat flow *versus* temperature for a DSC experiment on *t*-butanol. The sample was loaded as a liquid at room temperature. The temperature was scanned from 298 to 193 K and then cycled back to 313 K at a rate of 10 K min^{-1}. *A* = crystallization, *B* = phase transition from phase IV to phase II, *C*,*D* = anomaly due to a possible ordering of the methyl groups, *E* = phase transition from phase II to phase IV, *F* = melting.

Additionally, Atkins (1911) followed a similar annealing process and observed that the needle-like crystals of phase I, which are nucleated from the supercooled liquid, are transformed into crystals with a rhombohedral habitus (phase IV) if they are held at a temperature close to the melting point. Despite the prominence of *t*-butanol in the monoalcohol series, its wide use in chemistry as a solvent and its rich phase behaviour, it is only this phase, phase IV, that has so far had its structure determined (Steininger *et al.*, 1989; CSD refcode VATSAK). Steininger *et al.* (1989) used single-crystal X-ray diffraction techniques on a zone-refined sample to show that phase IV of *t*-butanol has a triclinic structure with the space group $P\overline{1}$ and that it is characterized by hydrogen-bonded helical chains of molecules arranged along the *a* axis of the unit cell. There are two of these helices in the unit cell (each composed of three symmetry-independent molecules) and they are related by the inversion centre.

Here we report the first crystal structure determination of phase II of *t*-butanol, at both low-temperature and high-pressure, where we have used a combination of single-crystal X-ray diffraction techniques and *ab initio* density-functional calculations. We find that the structure is trigonal with $P\overline{3}$ symmetry and is characterized by the formation of hydrogen-bonded hexamers. Although the structure of phase II is very different from that of phase IV, the calculations indicate that the alteration of the hydrogen bonding of the molecules from catemer to hexamer results in a relatively small increase in the enthalpy (3.859 kJ mol^{-1}) for the trigonal structure at ambient pressure. At 0.85 GPa, the difference in enthalpy between the two crystal structures is reversed (and increases in magnitude slightly to 13.314 eV per molecule), indicating that only a fairly modest pressure is required to make the structure of phase II the relatively more stable.

2. Experiment and *ab initio* calculations

Initially, the low-temperature phase behaviour of *t*-butanol was surveyed by differential scanning calorimetery (DSC) measurements. These results were obtained using a Perkin Elmer Pyris DSC 1. The sample of *t*-butanol was distilled and dried using a vacuum line and loaded as a liquid into a sealed aluminium pan. The procedure was carried out at a scan rate of 10 K min^{-1} from 293 to 193 K and then back to room temperature (Fig. 1).

Crystallization occurred at 280.6 K and was indicated by the large exothermic peak (event *A* in Fig. 1). The peak also has a small endothermic shoulder at 276.5 K. The next event is at 250 K on cooling (event *B*), where another exothermic change occurs, due to a structural phase transition. This is followed by another event at 238 K where there is a slight kink in the graph on both cooling and heating (events *C* and *D*). It is postulated that this feature is due to ordering in the sample – perhaps due

Table 1
Refinement statistics for the low-temperature (220 K) and high-pressure (0.85 GPa) structure determinations of the trigonal $P\bar{3}$ phase (phase II) of tertiary butanol.

	Low temperature	High pressure
Crystal data		
Chemical formula	$C_4H_{10}O$	$C_4H_{10}O$
M_r	74.12	74.12
Cell setting, space group	Trigonal, $P\bar{3}$	Trigonal, $P\bar{3}$
Temperature (K)	220 (2)	293 (2)
a, c (Å)	18.0946 (13), 8.4041 (9)	17.55 (2), 8.080 (10)
V (Å^3)	2383.0 (4)	2155 (4)
Z	18	18
D_x (Mg m^{-3})	0.930	1.028
Radiation type	Mo $K\alpha$	Mo $K\alpha$
No. of reflections for cell parameters	3699	16
θ range (°)	2.5–25	2–10
μ (mm^{-1})	0.06	0.07
Crystal form, colour	Cylinder, colourless	Cylinder, colourless
Crystal size (mm)	0.5 × 0.1 × 0.1	0.02 × 0.02 × 0.01
Data collection		
Diffractometer	Bruker SMART APEX	Enraf–Nonius CAD-4
Data collection method	ω scans	ω scans
Absorption correction	Multi-scan (based on symmetry-related reflections)	Multi-scan (based on symmetry-related reflections)
T_{min}	0.816	0.253
T_{max}	1.000	0.562
No. of measured, independent and observed reflections	12 157, 2818, 2217	1808, 1203, 550
Criterion for observed reflections	$I > 2\sigma(I)$	$I > 2\sigma(I)$
R_{int}	0.026	0.211
θ_{max} (°)	25.0	20.0
Range of h, k, l	$-21 \Rightarrow h \Rightarrow 21$ $-21 \Rightarrow k \Rightarrow 21$ $-10 \Rightarrow l \Rightarrow 4$	$0 \Rightarrow h \Rightarrow 13$ $-16 \Rightarrow k \Rightarrow 14$ $-4 \Rightarrow l \Rightarrow 7$
Refinement		
Refinement on	F^2	F^2
$R[F^2 > 2\sigma(F^2)]$, $wR(F^2)$, S	0.044, 0.131, 1.07	0.115, 0.295, 1.01
No. of reflections	2818	1203
No. of parameters	144	64
H-atom treatment	Constrained to parent site	Constrained to parent site
Weighting scheme	$w = 1/[\sigma^2(F_o^2) + (0.0783P)^2 + 0.0635P]$, where $P = (F_o^2 + 2F_c^2)/3$	$w = 1/[\sigma^2(F_o^2) + (0.1552P)^2]$, where $P = (F_o^2 + 2F_c^2)/3$
$(\Delta/\sigma)_{max}$	0.164	0.014
$\Delta\rho_{max}$, $\Delta\rho_{min}$ (e Å^{-3})	0.13, −0.13	0.33, −0.21
Extinction method	*SHELXL97*	None
Extinction coefficient	0.0000 (12)	–

to the ordering of the methyl groups. The X-ray diffraction data were collected at 220 K and we have assigned the phase in this temperature region as phase II to be consistent with the results of Oetting (1963), who found that phase II is stable below 281 K.

On heating from 193 K to room temperature, the kink in the scan at 235 K is observed, then an endothermic event at 267.3 K (event *E*). This is the phase change associated with the exothermic peak at 250 K (*i.e.* event *B*) on cooling, although there is some hysteresis observed in the sample. The melting curve of the sample is very shallow; the onset is just above the phase transition at 270 K and is completed some 20 K later at 290 K (event *F*). This is the region where Oetting (1963) identified three further phases in the sample; it is clear from this experiment that there are no further phase transitions above 268 K, although there may have been a mixture of solid and liquid which may have affected their experiments. Consequently, we tentatively assign events *B* and *E* to being due to a phase transition between phase II and phase IV.

2.1. Low-temperature study

A distilled sample of *t*-butanol was loaded into a capillary using a vacuum line in order to prevent exposure to air and therefore reduce the risk of contamination of water into the hygroscopic sample. The capillary, with an internal diameter of ∼ 0.1 mm, was mounted and centred on a Bruker SMART APEX diffractometer (Siemens, 1993; graphite monochromated Mo $K\alpha$ radiation) equipped with a cryogenic cooling system, initially set at 243 K, and a 25 W OHCD laser-assisted crystal grower (Boese & Nussbaumer, 1994). This initial temperature ensured that the polycrystalline sample was safely in the phase II region. Subsequently, the temperature was raised to just below the phase II to phase IV transition temperature, and the laser was used to establish a solid–liquid boundary. A single crystal was obtained by zone refinement of the sample over a time span of 20 min. A series of frames was collected both to assess the crystal quality and to provide an initial unit cell for the sample at the 268 K crystal growth temperature. The reflections were indexed using *GEMINI* (Sparks, 1999), and the crystal system was found to be trigonal. The sample was then cooled to 220 K, whilst monitoring the diffraction pattern every 10 K, to ensure that the event associated with points *C* and *D* in the DSC experiment did not degrade the sample quality. A hemisphere of data was collected using 20 s exposures and 0.3° scans in ω. This data set was indexed, integrated, solved and refined using *GEMINI* (Sparks, 1999), *SAINT* (Siemens, 1995) and the *SHELX* suite (Sheldrick, 1997). The H atoms were placed in idealized positions and the final refinement statistics are presented in Table 1.[1] (Although attempts were made to grow single crystals of phase I, the samples proved to be unstable, even when contained within capillaries, and we therefore limited the scope of this study to the determination of phase II.)

2.2. High-pressure study

At ambient conditions *t*-butanol is a crystalline solid, but on gentle heating it can be readily liquefied. The *t*-butanol sample was loaded and pressurized in a Merrill–Bassett diamond anvil cell (Merrill & Bassett, 1974), which had been warmed to a temperature just above the melting point of *t*-butanol and had been equipped with 600 µm culet diamond anvils and a

[1] Supplementary data for this paper are available from the IUCr electronic archives (Reference: WS5038). Services for accessing these data are described at the back of the journal.

Table 2
Lattice parameters (Å, °, Å^3) obtained from the *ab initio* density functional calculations for both the triclinic $P\overline{1}$ and the trigonal $P\overline{3}$ phases of tertiary butanol at 0 and 0.85 GPa.

	0 GPa	0.85 GPa
$P\overline{1}$		
a	6.2027	6.0631
b	9.1431	9.0661
c	14.7554	14.4493
α	86.373	85.248
β	78.776	78.531
γ	76.363	75.800
$V_{\rm cell}$	797.363	754.133
$V_{\rm molecule}$	132.894	125.689
$P\overline{3}$		
a	17.5898	17.4389
c	8.1014	8.0210
$V_{\rm cell}$	2170.755	2112.510
$V_{\rm molecule}$	120.598	117.362

tungsten gasket. After the nucleation of many crystallites the temperature was cycled close to the melting curve, in order to reduce the number of crystallites, in a manner similar to that adopted by Vos *et al.* (1992, 1993). Finally, a single crystal was obtained at approximately 0.85 (1) GPa that entirely filled the 250 µm gasket hole.

The setting angles of 17 strong reflections were determined on an Enraf–Nonius CAD-4 diffractometer (equipped with an Mo X-ray tube) and a least-squares fit to the data gave trigonal unit-cell parameters that compare closely with the unit-cell parameters measured at low temperature.

Intensity data were collected with the ω-scan method at the position of least attenuation of the pressure cell, according to the fixed-φ technique (Finger & King, 1978). All accessible reflections were measured in the shell $+h$, $\pm k$, $\pm l$ for $0\ \text{Å}^{-1} < \sin\theta/\lambda < 0.48\ \text{Å}^{-1}$. The intensities were corrected for absorption and then used for structure solution by direct methods in $P\overline{3}$ symmetry. Three molecules were identified in the asymmetric unit and the structure was refined with the *SHELX* suite of programs (Sheldrick, 1997). Owing to the low completeness of the high-pressure data set, the displacement parameters were refined isotropically. The H atoms were placed in idealized positions. The refinement statistics for the final fit are listed in Table 1.

2.3. *Ab initio* calculations

In order to acquire a fuller understanding of the relationship between the low-temperature and high-pressure phases, we have performed a series of *ab initio* calculations using the *CASTEP* code (Segall *et al.*, 2002). This also allows us to obtain accurate H-atom positions, which are difficult to obtain using X-ray diffraction techniques.

The calculations were performed using the density functional formalism with the generalized gradient approximation (Perdew & Wang, 1992) applied for the many electron exchange and correlation interactions. This approach is known to improve the description of the structural and electronic properties of hydrogen-bonded systems compared with the commonly used local density approximation (Perdew & Zunger, 1981). Non-local ultra-soft pseudopotentials generated by the method of Vanderbilt (1990) were used to describe electron-ion interactions. The valence electron wavefunctions were expanded in a plane-wave basis set with a kinetic energy cut-off of 540 eV. This converges the total energy of the system to better than 0.001 eV per molecule (0.096 kJ mol^{-1}). Brillouin zone integrations were performed on a Monkhorst–Pack grid (Monkhorst & Pack, 1976) that is large enough to reach a level of convergence in total energy similar to the wavefunction cut-off. The electronic structure calculation proceeds *via* a preconditioned conjugate gradients, energy-minimization scheme (Payne *et al.*, 1992) and density mixing algorithm using the plane-wave coefficients as variational parameters.

The experimentally determined atomic positions and lattice parameters were used in the calculations as a starting point, from which relaxed structural parameters were determined. The Hellmann–Feynman theorem was used to calculate the forces on the individual atoms, which were used to relax the structure. The *ab initio* stresses on the cell were also used to relax the cell parameters. We include a correction to the stresses and total energy (Francis & Payne, 1990) that is required since the basis set changes as the unit cell is optimized. However, our basis set is large enough that these corrections are very small and are only included for completeness.

3. Results and discussion

On performing the calculations to fully relax the structures of phase II and phase IV of *t*-butanol, we find that the lattice parameters are in good agreement with the experimental data (see Table 2). In the calculations, the symmetry of the structures was not constrained and we find that no symmetry breaking occurs during the calculations, indicating that they are in agreement with the experimentally determined space groups for both phases. The calculated fractional coordinates, including those for the H atoms, are also in excellent agreement with those determined experimentally (see deposited data). This gives us additional confidence that we have accurately determined the structure of phase II from the X-ray diffraction experiments and we have confirmed the structure of phase IV.

The pseudo-threefold nature of the molecular chains in phase IV of *t*-butanol is readily observed in an *a*-axis projection of the crystal structure, as shown in Fig. 2. Neighbouring chains are aligned alternately antiparallel to one another along the *a* axis and, in graph-set notation, these adopt a $C_3^3(6)$ configuration. The structure has three unique molecules in the asymmetric unit, which gives rise to three unique hydrogen bonds. The donor–acceptor distances, calculated from the structure reported by Steininger *et al.* (1989), are 2.714 Å for O1$\cdots$O3, 2.712 Å for O3$\cdots$O2 and 2.741 Å for O2$\cdots$O1($1+x, y, z$).

In phase II there are three symmetry-independent molecules and these form six-membered rings or hexamers, as shown in Fig. 3. In graph-set notation, both rings have the

notation $R_6^6(12)$, with six hydrogen bonds forming each ring. There are two unique hexamers within the structure, referred to as hexamer I and hexamer II. Hexamer I has one unique hydrogen bond and is centred at $(0, 0, \frac{1}{2})$. Hexamer II has two unique hydrogen bonds and is centred at $(\frac{2}{3}, \frac{1}{3}, 0.961\ (13))$ in the low-temperature structure and at $(\frac{2}{3}, \frac{1}{3}, 0.958\ (14))$ in the high-pressure structure. Hexamer I lies on a threefold roto-inversion centre, whereas hexamer II lies only on a threefold axis. Both hexamer I and hexamer II are arranged in the 'chair' conformation common to cyclohexane and its derivatives. Neighbouring *t*-butanol molecules are orientated either above or below the mean plane of the ring. Fig. 4 shows the packing arrangement of the hexamers within the phase II crystal structure in projection down the crystallographic *c* axis. Like phase IV of *t*-butanol, the asymmetric unit of phase II also contains three molecules, which again gives rise to three unique hydrogen bonds within the structure. The donor–acceptor distances for the low-temperature structure determination are 2.775 (1) Å for O1—O2(x, y, $z+1$), 2.779 (1) Å for O2—O1($-y+1$, $x-y$, $z-1$) and 2.729 (1) Å for O3—O3($x-y$, x, $-z+2$), while those for the high-pressure structure determination are 2.786 (9) Å for O1—O2(x, y, $z+1$), 2.720 (9) Å for O2—O1($-y+1$, $x-y$, $z-1$) and 2.698 (7) Å for O3—O3($x-y$, x, $-z+2$).

A measure of the flatness of the hexamers can be made by considering the torsion angle between four neighbouring O atoms in the ring. Hexamers I and II each have a characteristic torsion angle. In hexamer I, the torsion angle O3—O3(y, $y-x$, z)—O3($y-x$, $-x$, z)—O3($-x$, $-y$, $2-z$) is 50.1 (1)° at 220 K and reduces to 42.1 (7)° at 0.85 GPa. In hexamer II, the torsion angle O1—O2(x, y, $1+z$)—O1($1-y$, $x-y$, z)—O2($1-y$, $x-y$, $1+z$) is found to be 50.1 (1)° at 220 K, which reduces to 47.8 (5)° at 0.85 GPa. Hence, with pressure, there is a slight flattening of both hexamers.

Examining the crystal packing as a whole, one notable feature is the range of methyl–methyl contacts present. (All distances refer to the carbon–carbon separations.) Methyl groups on the same *t*-butanol molecule are separated by 2.48 Å on average. The intrahexamer contacts are 3.98 Å for hexamer I, and 4.01 and 4.20 Å for hexamer II. However, the interhexamer separations are significantly shorter, with a shortest methyl–methyl contact of only 3.52 Å. The methyl–

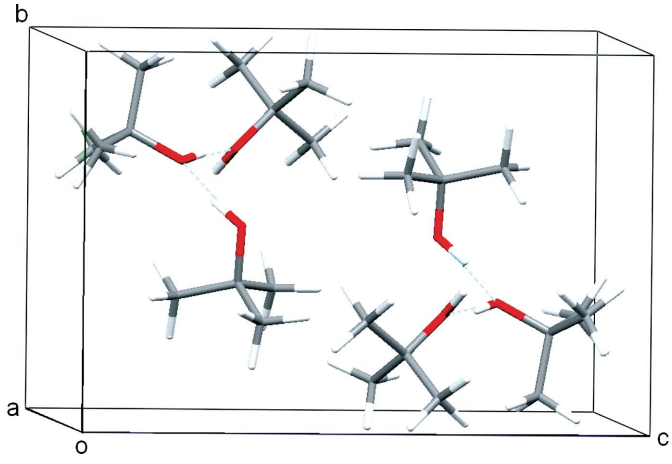

Figure 2
The crystal structure of the triclinic $P\overline{1}$ phase IV of *t*-butanol, viewed approximately along the crystallographic *a* axis. The threefold helical nature of the hydrogen-bonded molecular chains is apparent. The figure was generated using the unit-cell parameters and fractional coordinates from the 0 GPa calculation.

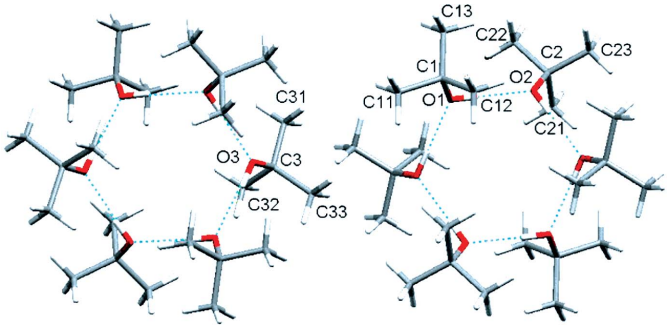

Figure 3
A projection along the crystallographic *c* axis of hexamer I and hexamer II in the trigonal $P\overline{3}$ phase II of *t*-butanol.

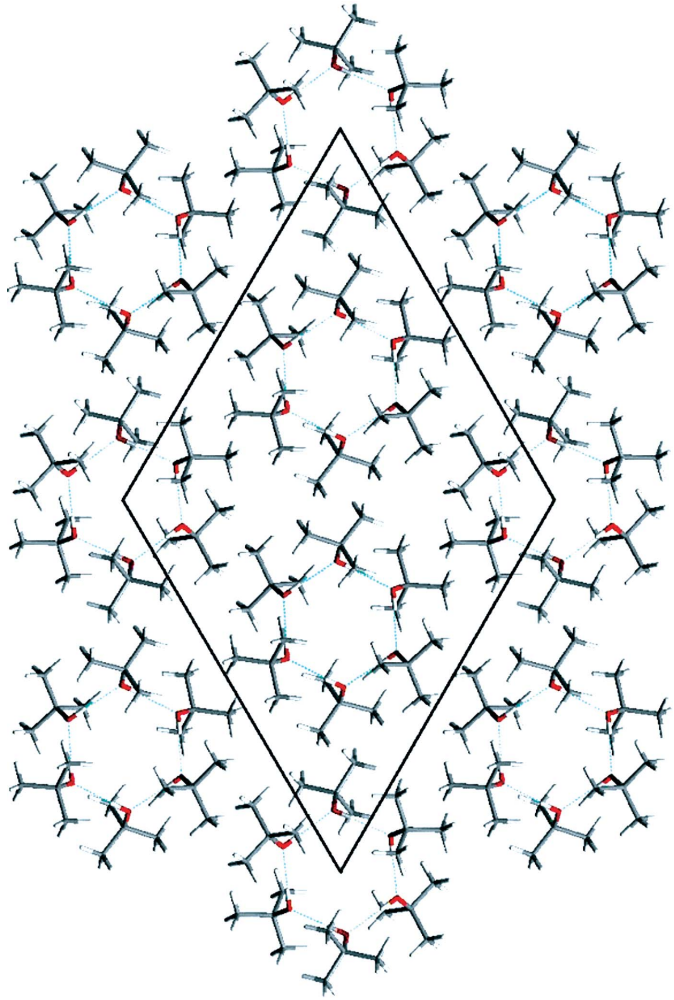

Figure 4
The crystal structure of the trigonal $P\overline{3}$ phase II of *t*-butanol viewed along the crystallographic *c* axis.

methyl contact motif is reminiscent of that of the low-temperature phase of acetic acid as the axes of the interacting methyl groups (defined by the C—C bonds) are approximately perpendicular to one another and are directed towards the methyl C atom of the adjacent interacting molecule (Allan & Clark, 1999). In the low-temperature phase of acetic acid the methyl–methyl contacts form a zigzag link between adjacent hydrogen-bonded catemers, while the inter-hexamer contacts of the high-pressure phase of *t*-butanol form the vertices of what are almost equilateral triangles arranged on layers parallel to the *xy* plane (Fig. 5*a*). The triangle formed by atoms C13, C23 and C33 is arranged on a layer at $z \simeq \frac{3}{4}$, and the triangle formed by atoms C11, C22 and C31 is formed on a layer $z \simeq \frac{1}{4}$.

In contrast, the interhelical methyl–methyl contact motif of low-temperature $P\overline{1}$ phase IV involves only individual pairs of molecules, on neighbouring helices. The axes defined by the C—C bond on each interacting methyl group lie along the line of contact and are almost ideally collinear to one another (Fig. 5*b*). This form of methyl–methyl interaction motif is very similar to that exhibited by the high-pressure phase of acetic acid, where the intercatemer contacts involve only individual pairs of molecules that have almost perfectly coincident molecular axes (Allan & Clark, 1999). The shortest interhelical methyl–methyl contacts for phase IV of *t*-butanol is 3.67 Å, which is significantly shorter than the intrahelical contacts of 4.05, 4.16 and 4.35 Å and marginally longer than the corresponding interhexamer distance in $P\overline{3}$ phase II.

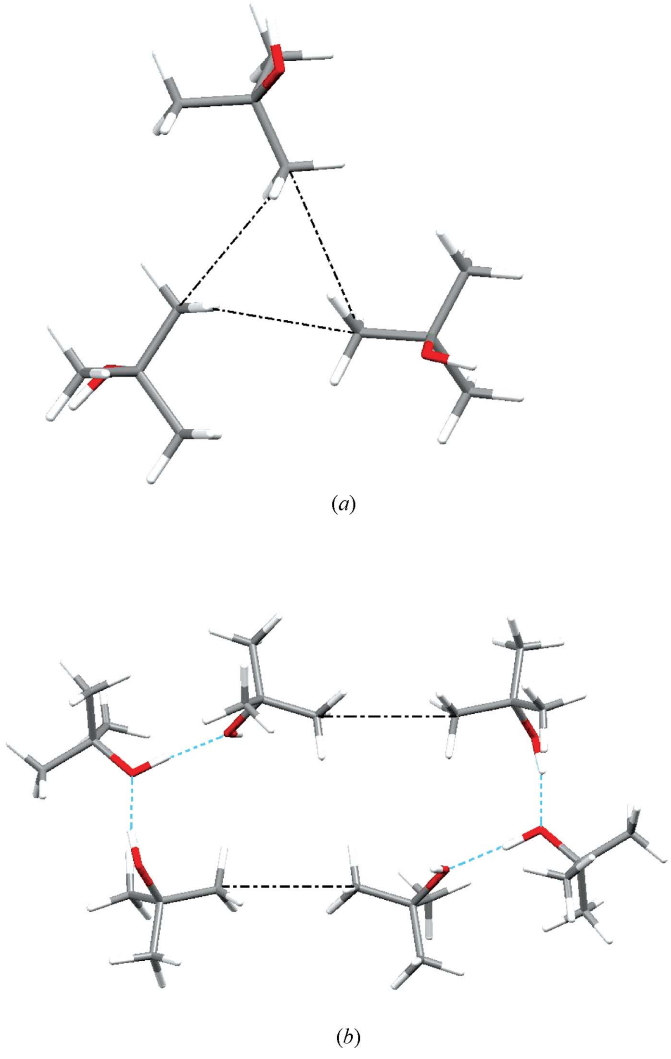

Figure 5
The methyl–methyl interactions (- · · · -) in (*a*) the trigonal $P\overline{3}$ phase II of *t*-butanol and (*b*) the triclinic $P\overline{1}$ phase IV of *t*-butanol.

We have been able to examine the relative energies of the phases at both ambient (0.0 GPa) and elevated pressure (0.85 GPa) using the first-principles techniques. The relative total energies per molecule give a measure of the relative stability of each phase, although this approach does not give an indication of barrier heights, which can be used to estimate thermal stability. At ambient pressure it is found that phase IV is more stable than phase II by 3.859 kJ mol^{-1}, while at elevated pressure the order of stability is reversed with a difference in enthalpy of 13.314 kJ mol^{-1}, indicating that the application of pressure acts to stabilize the trigonal phase II. Our calculations also reveal that phase II is denser than phase IV at both ambient pressure and 0.85 GPa (see Table 2), and this fact may partly explain why we found that phase II would crystallize in preference to phase IV in our ambient-pressure experiments. The difference in the calculated total energies at ambient pressure is certainly relatively small, and the crystallization of one phase in preference to another will strongly depend on the initial nucleation and variations in the crystal growth conditions. These effects, including the influence of crystal seeding on the particular phase grown at ambient pressure, have been documented by Steininger *et al.* (1989).

Although our calculations reveal that phase II is denser than phase IV at both ambient and elevated pressure (Table 2), our calculations reveal that the difference in relative energy at ambient pressure is fairly modest.

4. Conclusions

In conclusion, we have solved the trigonal $P\overline{3}$ phase II crystal structure of tertiary butyl alcohol, at both low-temperature and high-pressure, and find that this phase and the triclinic $P\overline{1}$ phase (phase IV) have very similar enthalpies despite the extremely substantial change of intermolecular bonding motif from helical catemer to hexamer. The hexamers in the trigonal phase adopt a chair conformation and at low temperature these are centred at (0, 0, $\frac{1}{2}$) and ($\frac{2}{3}$, $\frac{1}{3}$, 0.961 (13)), and at high pressure the centres are (0, 0, $\frac{1}{2}$) and ($\frac{2}{3}$, $\frac{1}{3}$, 0.958 (14)). Between these layers, the hexamers are linked by methyl–methyl contacts, which form nearly ideal equilateral triangles on layers at $z \simeq \frac{1}{4}$ and $z \simeq \frac{3}{4}$. The increased stability of phase II over that of phase IV with pressure, as indicated by the series of *ab initio* calculations, is contrary to the general trend towards small *R*-group behaviour that we have observed in the other members of the monoalcohol series. However, as the pressure range of the current study is extremely limited, we would certainly expect there to be additional polymorphs at higher pressure, which may have crystal structures consisting of relatively simple pseudo-twofold catemers in agreement

with the general structural trends that we have already observed.

We thank the EPSRC for funding this work and for supporting DRA through his EPSRC Advanced Research Fellowship.

References

Allan, D. R. & Clark, S. J. (1999). *Phys. Rev. B*, **60**, 6328–6334.
Allan, D. R., Clark, S. J., Brugmans, M. J. P., Ackland, G. J. & Vos, W. L. (1998). *Phys. Rev. B*, **58**, R11809–R11812.
Allan, D. R., Clark, S. J., Dawson, A., McGregor, P. A. & Parsons, S. (2002). *Acta Cryst.* B**58**, 1018–1024.
Allan, D. R., Parsons, S. & Teat, S. J. (2001). *J. Synchrotron Rad.* **8**, 10–17.
Atkins, W. R. G. (1911). *J. Chem. Soc.* **99**, 10–23.
Boese, R. & Nussbaumer, M. (1994). *Correlations, Transformations and Interactions in Organic Chemistry*, IUCr Crystallographic Symposia, Vol. 7, edited by D. W. Jones & A. Katrusiak. Oxford University Press.
Brock, C. P. & Duncan, L. L. (1994). *Chem. Mater.* **6**, 1307–1312.
Finger, L. W. & King, H. (1978). *Am. Mineral.* **63**, 337–342.
Francis, G. P. & Payne, M. C. (1990). *J. Phys. Condens. Matter*, **2**, 4395–4404.
McGregor, P. A., Allan, D. R., Parsons, S. & Pulham, C. R. (2005). *Acta Cryst.* B**61**, 449–454.
Merrill, L. & Bassett, W. A. (1974). *Rev. Sci. Instrum.* **45**, 290–294.
Moggach, S. A., Allan, D. R., Parsons, S., Sawyer, L. & Warren, J. E. (2005). *J. Synchrotron Rad.* **12**, 598–607.
Monkhorst, H. J. & Pack, J. D. (1976). *Phys. Rev. B*, **13**, 5188–5192.
Neu, W. J.-M. (1968). *C. R. Acad. Sci. Paris Ser. C*, **267**, 1025–1028.
Oetting, F. L. (1963). *J. Phys. Chem.* **67**, 2757–2761.
Oswald, I. D. H., Allan, D. R., Day, G. M., Motherwell, W. D. S. & Parsons, S. (2005). *Cryst. Growth Des.* **5**, 1055–1071.
Oswald, I. D. H., Allan, D. R., Motherwell, W. D. S. & Parsons, S. (2005). *Acta Cryst.* B**61**, 69–79.
Payne, M. C., Teter, M. P., Allan, D. C., Arias, T. A. & Joannopoulos, J. D. (1992). *Rev. Mod. Phys.* **64**, 1045–1097.
Perdew, J. P. & Wang, Y. (1992). *Phys. Rev. B*, **45**, 13244–13249.
Perdew, J. P. & Zunger, A. (1981). *Phys. Rev. B*, **23**, 5048–5079.
Sciesinska, E. & Sciesinska, J. (1980). *Acta. Phys. Pol. A*, **58**, 361–368.
Segall, M. D., Lindan, P. J. D., Probert, M. J., Pickard, C. J., Hasnip, P. J., Clark, S. J. & Payne, M. C. (2002). *J. Phys. Condens. Matter*, **14**, 2717–2744.
Sheldrick, G. M. (1997). *SHELXL*97. University of Göttingen, Germany.
Siemens (1993). *SMART*. Siemens Industrial Autom. Inc., Madison, Wisconsin, USA.
Siemens (1995). *SAINT*. Siemens Industrial Autom. Inc., Madison, Wisconsin, USA.
Sparks, R. A. (1999). *GEMINI*. Bruker AXS Inc., Madison, Wisconsin, USA.
Steininger, R., Bilgram, J. H., Gramlich, V. & Petter, W. (1989). *Z. Kristallogr.* **187**, 1–13.
Vanderbilt, D. (1990). *Phys. Rev. B*, **41**, 7892–7895.
Vos, W. L., Finger, L. W., Hemley, R. J., Hu, J. Z., Mao, H. K. & Schouten, J. A. (1992). *Nature* (*London*), **358**, 46.
Vos, W. L., Finger, L. W., Hemley, R. J. & Mao, H. (1993). *Phys. Rev. Lett.* **71**, 3150–3153.